Water Model Experiments on the Influence of Phase Distribution in the Submerged Entry Nozzle Considering Varying Operating Conditions

Maria Thumfart, Gernot Hackl, and Wolfgang Fellner*

Continuous casting of steel argon injection into the submerged entry nozzle (SEN) via the stopper is common practice. Nonetheless, the resulting phase distribution in the SEN is still under discussion. The main available casting parameters at the steel plant to determine the flow situation in the SEN are usually the stopper rod position, the argon feeding pressure, the argon flow rate, and the casting speed. To show the potential influence of the phase distribution on the stopper characteristic and on the argon feeding pressure, experiments using a 1:3 scale water model are presented. For the experiment, the water flow rate is scaled using Froude similarity, while the air flow rate is chosen to keep the ratio between the liquid and gas volume flow rate constant. The casting parameters and the pressure at three distinct levels of the SEN are measured. To relate this measurement data to the corresponding phase distribution, two cameras are used to document the phase distribution in the SEN. The images show four major phase distribution patterns. These patterns can be linked to significant changes in the measured pressure levels and the behavior of the stopper.

1. Introduction

In the continuous casting of steel, a stopper rod is a widely used device to control the steel flow rate from the tundish to the mold. It is common practice to inject argon at or near the stopper tip to reduce clogging in the submerged entry nozzle (SEN).[1] This argon injection leads to a complex two-phase flow situation in the SEN. The interface between steel and argon can collect nonmetallic particles and trigger degassing of the steel. It changes the necessary stopper lift at a given steel flow rate and the resulting gas bubbles can change the flow pattern in the mold. In addition, the argon injection changes the pressure distribution in the SEN, which directly influences the air aspiration rate.[2,3] All these aspects are strongly influenced by the phase distribution (steel argon) in the SEN.

The phase distributions possible in concurrent downward gas liquid flows have already been thoroughly investigated.[4–7] These investigations show that the phase distribution can range from bubbly, slug, and churn to annular flow. Research showed the large impact of the inflow boundary condition on the observed phase distribution in a concurrent downward gas liquid flow in experiments with a pipe length of more than 200 pipe diameters.[8,9] Accordingly, the flow situation in the SEN which has a length of ≈14 pipe diameters needs to be assumed to be completely dominated by the inflow boundary condition. Thus, investigations on a straight pipe[10] can only be used to investigate some isolated effects but not the flow situation in the SEN.

The phase distributions possible in the SEN at continuous casting plants are still subject of ongoing investigations.[11–13] There are mainly three approaches to investigate these phase distributions: measurements directly at the continuous casting plant, physical models operated with metals melting at lower temperatures or water, and computational fluid dynamics (CFD) simulations. Each approach has its own set of limitations.

At the continuous casting plant, measurements of the stopper position, the stopper feeding pressure, the argon flow rate, and the casting speed (i.e., the steel mass flow rate), as well as the tundish and mold level are often available. Additional measurements of the phase distribution are difficult to execute and are often hard to interpret.[14] They cannot be performed at the upper part of the SEN due to the thick tundish lining. So, the conditions near the stopper tip can only be determined from the stopper lift and the argon backpressure.

Physical models filled with liquid metal are more accessible.[14–17] Their surface tension and liquid density match the conditions of liquid steel very well. Thus, the bubble sizes and the pressure distribution in the SEN can be assumed to be in very good agreement with the situation in the continuous caster. Nonetheless the liquid metal is still opaque and can reach up to 170 °C, so the operation of

M. Thumfart
Area 4
K1-MET GmbH
Stahlstraße 14, A-4020 Linz, Austria
E-mail: maria.thumfart@k1-met.com

G. Hackl, W. Fellner
Global Engineering & Simulations
RHI Magnesita GmbH
Magnesitstr. 2, A-8700 Leoben, Austria

The ORCID identification number(s) for the author(s) of this article can be found under https://doi.org/10.1002/srin.202100824.

DOI: 10.1002/srin.202100824

these physical models is a demanding task and the methods to detect the phase distribution are still limited.[15,16]

Physical models filled with water are easier to handle. However, the surface tension of water is far below that of liquid steel and the density is ≈1/7. So, the results from water models cannot be transferred directly to steel plant conditions in case of gas injection. As they can be built as completely transparent, the phase distribution in the SEN can be observed directly and changes in the wetting conditions can be easily achieved. So, water models can for instance be used to show the impact of phase distribution in the SEN on parameters like the stopper lift or pressure distribution. They as well allow to show the qualitative impact of changes in the wetting conditions near the argon injection position on the behavior of the system.

CFD models are able to capture the flow situation if the phase distribution is known. In case of large gas volumes with respect to geometry, the volume of fluid can be used. In case of small bubbles, the discrete particle model or Euler–Euler model leads to satisfying results.[18] However, if it comes to phase distribution transitions, they still have limited capacities.[19–21]

Ideally, plant measurements, physical models, and CFD models complement each other. The results from physical models can facilitate the interpretation of the process data from the continuous casting plant or can be used for CFD model validation. These models can then further be used to investigate the flow situation in more detail or be adapted to the flow situation of the steel plant. The data from the steel plant can be used as a benchmark as well and narrow down the types of flow phenomena observed in the modeling attempts to be further investigated.

The focus of the research presented in this article is the influence of the phase distribution in the SEN on the stopper lift and on the pressure at the stopper tip. In case of this study, a 1:3 scale water model is used. To isolate the impact of the phase distribution from the impact of the water and air flow rates, a hysteresis effect and the influence of different wetting conditions at the stopper tip are exploited to reach up to three different phase distributions at the same set of flow rates.

2. Experimental Section

The setup used for the experiments presented in this article is shown in **Figure 1**. It is a 1:3 water model of a continuous caster and is run by RHI Magnesita. The 1:3 water model is a downscaled version of the 1:1 water model which has been studied in the past.[22] The left image shows an overview of the whole setup, while the sketch in the center shows the available measurement data. The two photographs at the right show images of the upper and lower part of the SEN.

The water entered the tundish in a side chamber and flows into its main part through a perforated wall. The stopper was mounted on a float which controls the tundish fill level. The water flowed past the stopper, through the SEN, and into the mold. The mold level was controlled by the geometry of the side chambers of the mold. From there the water exited the experimental setup. The air was injected at the stopper tip through a single nozzle at the center of the stopper tip.

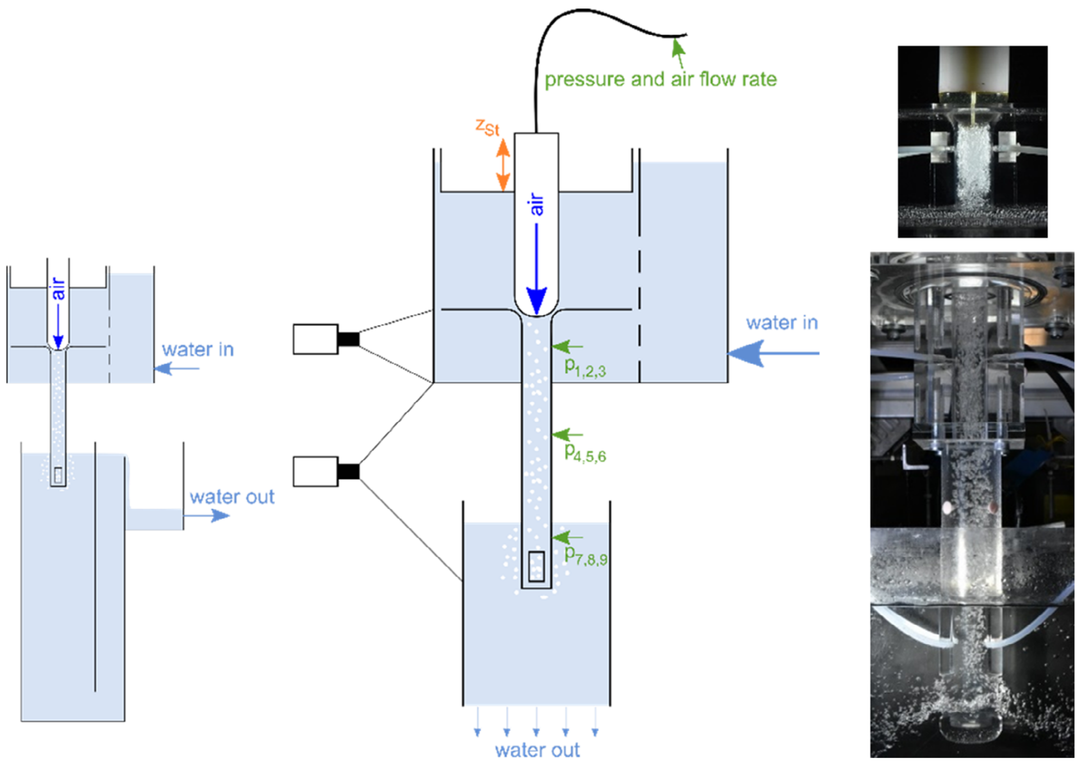

Figure 1. Experimental setup; left: overall view of setup; center: detailed information on the available measurements; right: images of the upper and lower part of the SEN.

Table 1. Used sensors.

value	Symbol	Sensor
Air flow rate	$\dot{V}_{air}$	FC-TECHNIK ag, MFM 8249
Water flow rate	$\dot{V}_{water}$	KROHNE OPTIFLUX 4000 F
Stopper position	z_{st}	WayCon LRW2-C-75
Stopper feeding pressure	p_{st}	Keyence AP-32P
SEN pressure	p_{SEN}	BD-Sensors DMP331 110-S200-1-3-100-300-1-000

The setup was transparent. To improve the visual accessibility of the upper part of the SEN, it was mounted within the original tundish at an elevated position. A second, thin tundish bottom was installed. Two cameras took pictures of the upper and lower part of the SEN at 1 Hz.

Nine pressure sensors were used to measure the SEN pressure at three different positions along the SEN length. They were arranged at a respective angle of 90°. The measurement lines were filled with water. Their respective height above the meniscus was 250, 120, and −20 mm. In addition, the air flow rate and the back pressure in the air feeding line, as well as the stopper position, were measured at 10 Hz. **Table 1** summarizes the used sensors.

The contact angle of air, water, and the wall at the stopper tip and near the stopper rod gap is an important parameter for phase distribution. To vary the contact angle, three different wall conditions were used: 1) Clean acrylic glass: The SEN and stopper were new; 2) Petrol jelly: The top part of the SEN (5 cm) and the stopper tip were coated with a thin layer of petrol jelly; and 3) Paraffin: The petrol jelly was removed and replaced by a thin layer of paraffin

3. Theoretical Considerations

Physical models are common practice in the research of metallurgical flows. The key issue in physical modeling is the correct scaling of the experimental setup. In the case of single-phase flow, the Reynolds and the Froude similarity are relevant. Reynolds similarity leads to similar turbulence, while Froude similarity leads to a similar ratio of inertial and gravitational forces. This leads to comparable meniscus deformations and a comparable stopper lift. With a 1:1 water model, both similarities can be met. With a 1:3 water model, on the other hand, only one of these similarities can be fulfilled. The experiments presented in this article are based on Froude similarity, to ensure a comparable stopper lift.

The Froude number calculates to

$$\mathrm{Fr} = \frac{U}{\sqrt{Lg}} \tag{1}$$

with the characteristic velocity U, the length scale L, and the gravitational acceleration g. Keeping the Froude number constant results in a velocity ratio of

$$\frac{U_m}{U_p} = \sqrt{\frac{L_m}{L_p}} = \sqrt{\frac{1}{3}} \tag{2}$$

with the model characteristic velocity being U_m, the plant characteristic velocity U_p, the model length scale L_m, and the plant length scale L_p. This velocity scale is used for liquid and gas phase. Accordingly, all volume flow rates in the 1:3 water model can be calculated from

$$\dot{V}_m = \dot{V}_p \frac{U_m}{U_p} \left(\frac{L_m}{L_p}\right)^2 = \dot{V}_p \frac{1}{9}\sqrt{\frac{1}{3}} \tag{3}$$

with the volume flow rate in the plant being $\dot{V}_p$, the model velocity scale U_m, the plant velocity scale U_p, the model length scale $L_{m,}$ and the plant length scale L_p.

To apply Equation (3) to the gas flow rate, the actual gas flow rate in the plant needs to be estimated. The ideal gas law is

$$\frac{p}{\rho} = RT \Rightarrow \rho = \frac{p}{RT} \tag{4}$$

with the gas pressure being p, the gas density ρ, the specific gas constant R, and the gas temperature T. Usually, the gas flow rate injected at the stopper tip in a steel plant is measured considering norm conditions (temperature T_{norm} and pressure p_{norm}). To calculate the actual gas flow rate, the pressure and temperature at the upper part of the SEN need to be taken into account accordingly.

$$\dot{V}_{Ar} = \dot{V}_{Ar,norm} \frac{p_{norm}}{T_{norm}} \frac{T_{stopper\,tip}}{p_{stopper\,tip}} \tag{5}$$

with the actual gas flow rate as $\dot{V}_{Ar}$, the gas flow rate at norm conditions as $\dot{V}_{Ar,norm}$, the temperature at the stopper tip as $T_{stopper\,tip}$, and the pressure at the stopper tip as $p_{stopper\,tip}$. This results in additional terms for the scaling law of the air flow rate in the model

$$\dot{V}_{air} = \dot{V}_{Ar} \frac{U_m}{U_p} \left(\frac{L_m}{L_p}\right)^2 = \dot{V}_{Ar,norm} \frac{p_{norm}}{T_{norm}} \frac{T_{stopper\,tip}}{p_{stopper\,tip}} \frac{1}{9}\sqrt{\frac{1}{3}} \tag{6}$$

In Equation (6), the values of the temperatures and the pressure at norm conditions are well-known constants. The only value to be estimated is the pressure at the stopper tip $p_{stopper\,tip}$. This can only be approximated, as the stopper tip pressure strongly depends on the phase distribution within the whole SEN. The most obvious estimate is the static pressure at the stopper tip

$$p_{stopper\,tip} = p_0 - \rho_{st}\, g\, h_{stopper\,tip} \tag{7}$$

with the ambient pressure being p_0, the steel density ρ_{st}, the gravitational acceleration g, and the height difference between the stopper tip and the meniscus $h_{stopper\,tip}$.

Both the temperature ratio (norm to stopper tip conditions) and the pressure ratio lead to an increase in the actual gas flow rate at the stopper tip. The temperature ratio is ≈6 and the pressure ratio is ≈3 (with $h_{stoper\,tip} \approx 0.8\,\mathrm{m}$). Using these assumptions, the air flow rate in the model simplifies to

$$\dot{V}_{air} = \dot{V}_{Ar,norm}\, 2\sqrt{\frac{1}{3}} \tag{8}$$

The air flow rate of the experimental setup can be approximated using the air flow rate at norm conditions as the temperature and pressure in the water model are close to norm conditions.

4. Results

The main goal of the experiments presented in this article is to show the influence of different phase distributions in the SEN on the flow parameters. To achieve different phase distributions at the same water and air flow rates, two different approaches are used: wetting conditions and a hysteresis effect at increasing and decreasing air flow rates.

4.1. Wetting Conditions

As already mentioned in Section 2, three different surface conditions are used to achieve different wetting behaviors. For these three conditions, the contact angle of a sitting drop is summarized in **Table 2**. In case of the acrylic glass, it was measured on a sample stored in dry conditions and on a sample resting in water for a week and then shortly dried. The measured difference of more than 10° indicates that the exposure time of the acrylic glass to water needs to be documented if the contact angle is a relevant parameter in a measurement campaign. In the presented cases, the exposure time is three days. The measured contact angles are well within the reported range on contact angles between liquid steel and refractory material.[23]

4.2. Flow Rates

As mentioned in Section 3, the flow rates in the 1:3 water model need to be scaled. The water flow rate is kept constant during each experiment, while the air flow rate is ramped up or down. The used flow rates are summarized in **Table 3**. The corresponding range of casting speed is approximately from 2.5 to 3.5 $\mathrm{t\,min^{-1}}$. The corresponding argon flow rate is approximately from 8 to 90 $\mathrm{L\,min^{-1}}$. This large gas flow rate is necessary to approximate the influence of low pressure at the stopper tip, as mentioned in Section 3.

Table 2. Measured contact angles.

Material	Contact angle [°]
Acryllic glass dry	90
Acryllic glass prev. wet	78
Petrol jelly	93
Paraffin	101

Table 3. Water and air flow rate in the experiments.

Material	Water flow rate [$\mathrm{l\,min^{-1}}$]	Air flow rate ramp up [$\mathrm{l\,min^{-1}}$]	Air flow rate ramp down [$\mathrm{l\,min^{-1}}$]	Figures
Acrylic glass	32	0.5–5.8	5.8–0.5	3,4(1),5(1)
Acrylic glass	28	0.5–5.8	5.8–0.5	4(2),5(2)
Petrol jelly	28	0.5–5.8	5.8–0.5	4(3),5(3)
Paraffin	28	0.5–5.8	5.8–0.5	4(4),5(4)

4.3. Phase Distributions

Figure 2 shows schematic representations and example images of the observed phase distributions during the experiments. As fresh tap water is used for the experiments, small bubbles form during each experiment at the outside of the top part of the SEN: (a) Bubble threads: The bubbles are arranged in narrow threads at the centers of vertically aligned vortices in the SEN. The bubbles inside the SEN are subject to motion blurring, while the ones sitting at the outside of the SEN are perfectly sharp. (b) Bubble foam: A dense layer of bubbles is visible near the wall. Everything behind it is obscured by the bubbles near the SEN wall. While in case (a) the back of the SEN is still visible, it is now completely obscured by bubbles (c) Intermediate level, air near wall: A large air pocket forms in the upper part of the SEN. The walls of the SEN in this upper part are dry. The air from the stopper tip plunges through the water jet. At some point this water jet impinges on the filled part of the SEN. The rest of the SEN exhibits a bubbly flow. In the example image, the yellow arrow indicates the upper end of the large air pocket. Downward from this air pocket the wall is dry. The difference in the refractory index between acrylic glass and air is significantly larger than the difference between acrylic glass and water. Thus, the light path changes significantly which leads to this strong increase in brightness. (d) Intermediate level, air in the center: The water flows down at the SEN walls and the air forms a large volume in the center of the SEN. Compared with case (c) this gas volume is much longer. It can reach the end of the SEN where big portions can exit periodically. In the example image, the region near the stopper tip (top 5 mm) looks similar to case (c). Nonetheless, the difference between case (c) and case (d) is clearly visible in the lower part of the photograph.

The phase distributions (a), (b), and (c) all result in small bubbles in the lower part of the SEN. They can only be visually distinguished near the stopper tip. They, however, result in different pressure and stopper position measurements. This can be observed in the videos included in Supporting Information. The phase distributions have been identified visually by reviewing these videos.

Figure 3 shows the measurement results of two ramps using the clean acrylic glass setup. Both ramps have a duration of 30 min. This example contains all four phase distributions observed during the experiments. The identified phase distributions are indicated in the graph of the pressure at the stopper tip p_{StTip} and the graph of the stopper position z_{st}. The yellow and purple lines in the graph of the pressure along the SEN p_{SEN} show the pressure measured without gas injection. The green and cyan lines in the stopper position diagram (z_{st}) show the result of a moving average of 5 s.

In case of bubble threads (a), the pressure at the stopper tip p_{StTip} reaches a high level. When it changes to bubble foam (b), the pressure p_{StTip} drops, and the stopper position z_{st} drops as well. The fluctuation level stays the same. When the phase distribution changes to intermediate level, air centered (d), the pressure at the stopper tip p_{StTip} rises to almost the same level as in

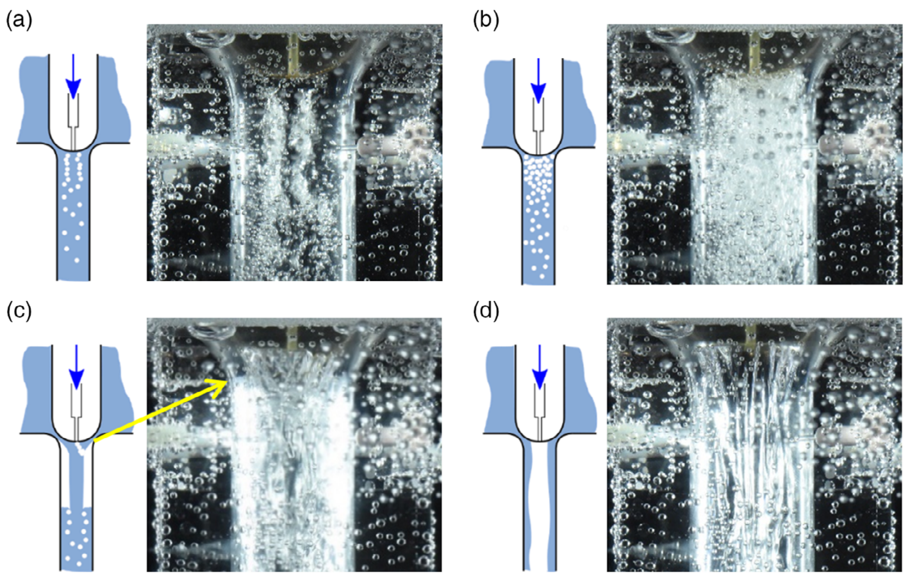

Figure 2. Sketches and example images of the observed phase distribution patterns: a) Bubble threads: bubbles arranged in the centers of vertical vortices. b) Bubble foam: bubbles near the SEN wall are too dense to see the background. c) Intermediate level, air near wall. d) Intermediate level, air centered.

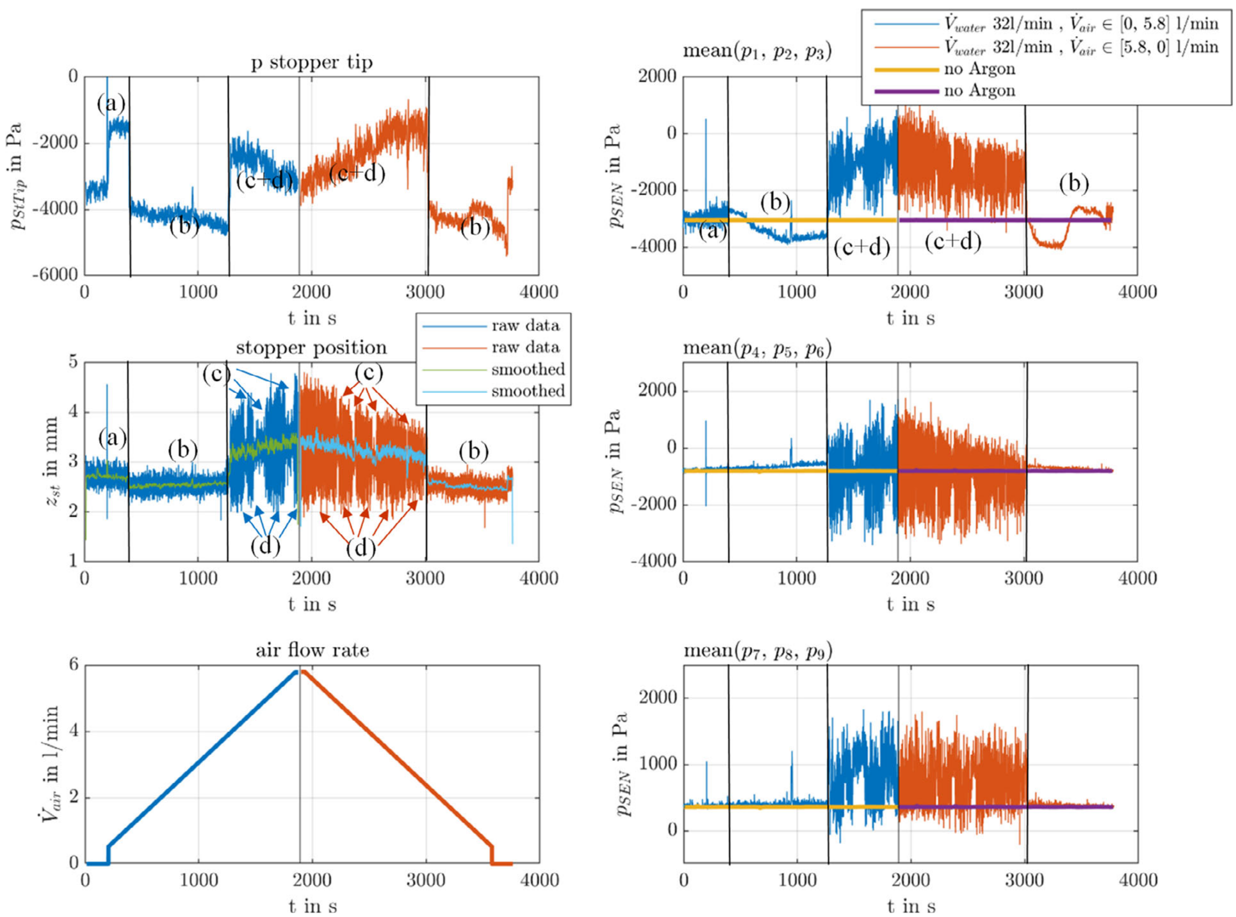

Figure 3. Examples of two measurements using clean acrylic glass. Blue line: increasing air flow rate. Red line: decreasing air flow rate; yellow and purple line: the SEN pressures without gas injection; variables: p_{StTip} pressure at the stopper tip calculated from the feeding pressure and the air flow rate, z_{st} stopper position, $\dot{V}_{air}$ air flow rate, and p_{SEN} average pressure of the three pressure sensors at each level in the SEN. The letters indicate the respective phase distributions described in Figure 2.

case of bubble threads (a). The average stopper position z_{st} rises and the fluctuation in the stopper tip pressure rises slightly, while the stopper position fluctuations rise significantly. In this state, the gas volume in the center of the SEN can reach the end of the SEN. Further increasing air flow rate, the phase distribution changes from (d) to (c) back and forth. This is mainly visible in the fluctuation magnitude of the stopper position. An intermediate level, air centered (d), leads to large fluctuations of the stopper position, while an intermediate level, water centered (c), leads to smaller fluctuations of the stopper position.

At decreasing air flow rate (red line Figure 3), an intermediate level $(c+d)$ can be observed until $t = 3010$ s. It again changes between case (c) and (d). This indicates that the exact flow rate at which case (c) or case (d) occurs is a stochastic process.

At $t = 3010$ s, the phase distribution changes to bubbly foam (b). This phase distribution becomes thinned out and starts to fluctuate at $t = 3350$ s but does not change back to bubble threads (a) within the available air flow range. This shows that both major phase distribution changes observed in this measurement show a hysteresis effect. Within the hysteresis region, the only remaining parameter to explain the different pressure and stopper position values is the phase distribution.

The pressure in the SEN p_{SEN} is shown in the right column in Figure 3. The three pressure signals at each level are averaged in each respective figure. The average pressure at the top measuring level $p_{1,2,3}$ shows significant differences for all phase distributions. In case of bubble threads (a), the time average of the pressure is only slightly above the single-phase pressure (yellow line) and shows significant fluctuations; in case of bubble foam (b), the pressure starts slightly above the single-phase pressure and then drops below it. In case (b), the pressure fluctuations are significantly smaller compared with case (a). When the phase distribution changes to intermediate level $(c+d)$, the pressure increases considerably alongside the fluctuation magnitude. The pressure fluctuations are smaller for case (d) compared with case (c).

The average pressure at the middle and lower level ($p_{4,5,6}$ and $p_{7,8,9}$) does not show any difference between bubble threads (a) and bubble foam (b), while the difference to intermediate level $(c+d)$ is clearly visible. The difference between the two types of

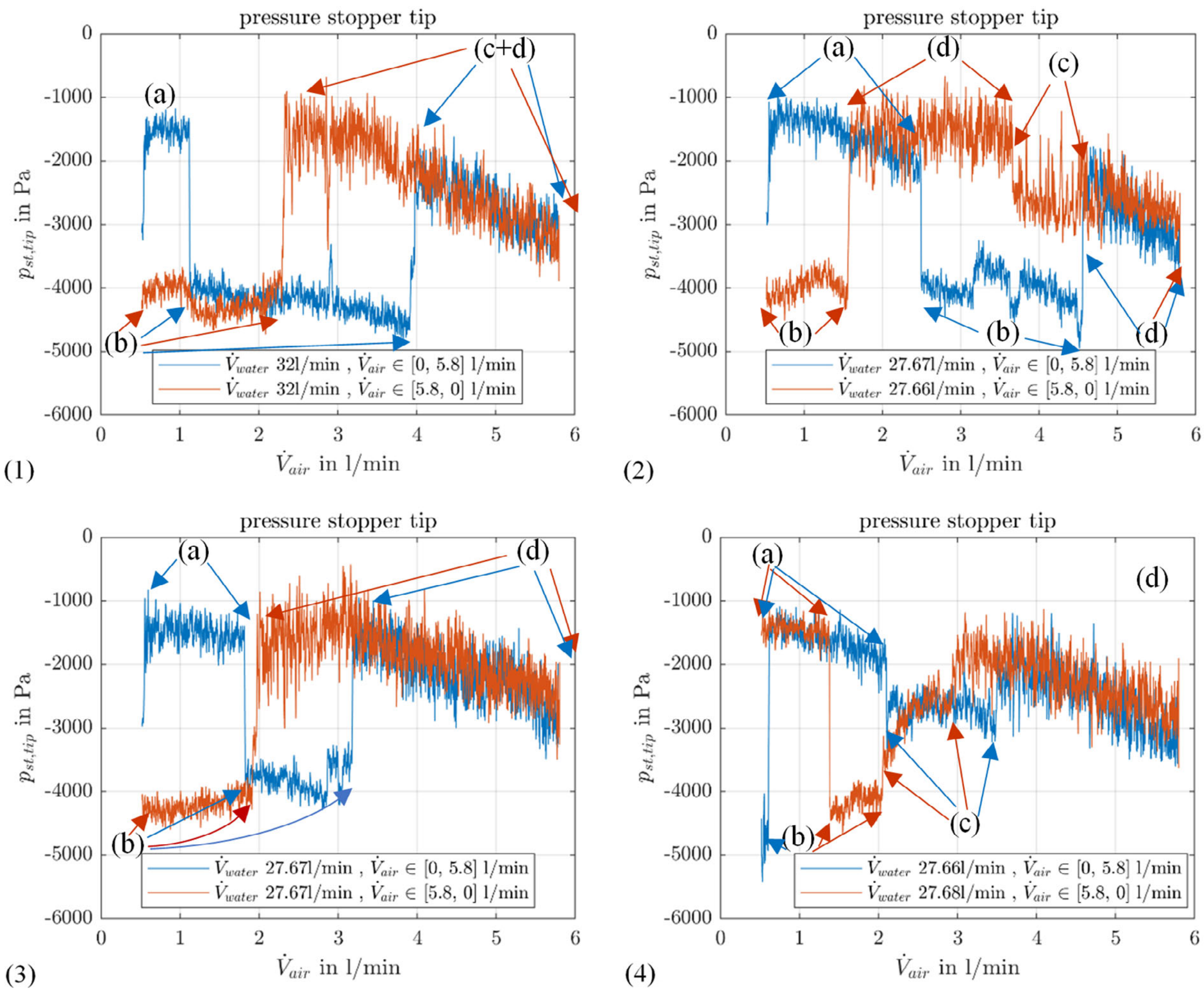

Figure 4. Stopper tip pressure; arrows indicate start and end of the respective phase distributions (assigned letters according to Figure 2); arrow color matches line color; The letters indicate the respective phase distributions described in Figure 2. (1) water flow rate: 32 L min^{-1}, acrylic glass; (2) water flow rate: 28 l min^{-1}, acrylic glass; (3) water flow rate: 28 l min^{-1}, petrol jelly; (4) water flow rate: 28 l min^{-1}, paraffin.

intermediate levels is the fluctuation magnitude of the pressure signals. This indicates that the difference in the flow field at this level between bubble threads (a) and bubble foam (b) is already marginal.

In addition to the data in Figure 3, four videos of the observed phase distributions in the SEN are provided in the supplementary material. These four videos together cover the first 1800 s of the data in Figure 3 and contain the stopper feeding pressure p_{ST}, the stopper position z_{ST}, and the air flow rate $\dot{V}_{air}$. In the video a short change in the volume fraction of air at the end of the SEN can be observed at $t = 950$ s. This change of air volume fraction leads to a small pressure peak. The video as well shows the length difference of the large gas pocket between case (c) and (d). While the gas pocket length is almost constant in case (c), it fluctuates strongly in case (d). In case (d), it can even reach the outlet ports.

The results in Figure 3 already show that the jumps in the stopper lift z_{st} and the stopper tip pressure p_{StTip} at points of phase distribution changes are larger than the change of these values within one segment of constant phase distribution. For instance, the change in stopper tip pressure at an air flow rate from 1 to almost 4 L min^{-1} is about 200 Pa (blue line, (b)) while the jump at 4 L min^{-1} is about 2000 Pa. So, the impact of phase distribution exceeds the impact of the air flow rate.

Figure 4(1) and **5**(1) show the stopper tip pressure and the smoothened stopper position of the example in Figure 3 at a water flow rate of 32 L min^{-1}. The blue lines in all graphs in Figure 4 and 5 refer to increasing air flow rate with respect to time. The red lines in all graphs refer to decreasing air flow rate with respect to time. The letters indicate the observed phase distribution as shown in Figure 2. The arrows point to the respective starting and end points of the observed phase distributions. The colors of these arrows correspond to the respective curves.

While Figure 4(1) and 5(1) show the measurement results at 32 L min^{-1}, Figure 4(2,3,4) and 5(2,3,4) show measurements at 28 L min^{-1}. These three cases differ in wetting conditions. The detailed data for these cases are provided in the supplementary material (Figure S1 to S3, Supporting Information).

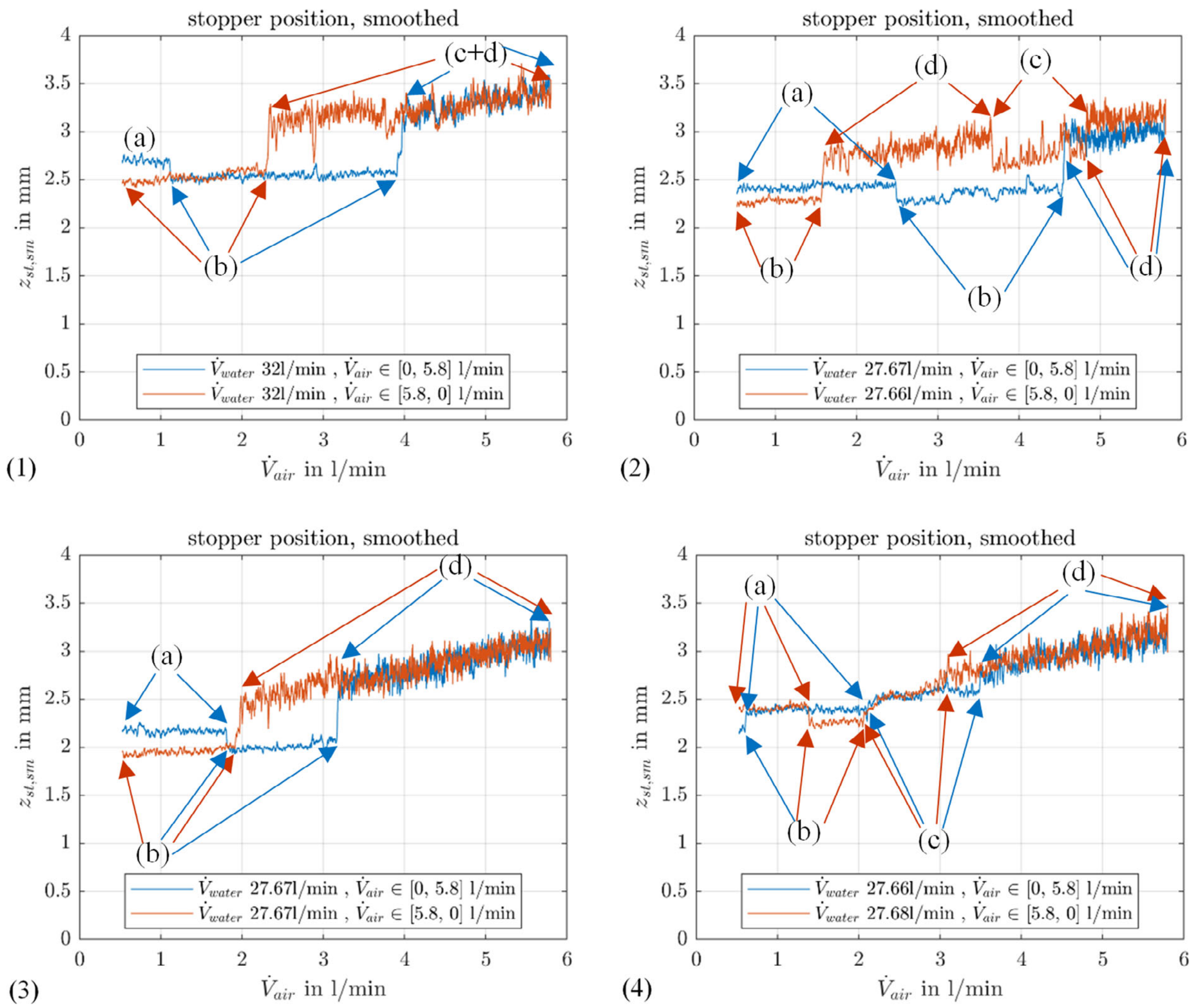

Figure 5. Smoothened stopper position; arrows indicate start and end of the respective phase distributions (Figure 2); color arrows match line color; The letters indicate the respective phase distributions described in Figure 2. (1) water flow rate: 32 l min^{-1}, acrylic glass; (2) water flow rate: 28 l min^{-1}, acrylic glass; (3) water flow rate: 28 l min^{-1}, petrol jelly; (4) water flow rate: 28 l min^{-1}, paraffin.

Accordingly, the comparison of Figure 4(1) with (2) shows the impact of the water flow rate on the results, while a comparison of Figure 4(2) with (3) and (4) shows the impact of up to three different phase distributions at one distinct pair of air and water flow rates. This is the case at an air flow rate of $3\,\mathrm{L\,min^{-1}}$. Figure 4(2) shows the results for bubbly foam (b) and intermediate level, air centered (d). Figure 4(4) shows the case of intermediate level, water centered (c).

In Figure 4(2), the stopper tip pressure at increasing air flow rate (blue line) during the condition of bubble foam (b) rapidly changes its level three times. These changes can be correlated to a change in gas holdup at the end of the SEN. These changes marginally affect the stopper position as well. The same effect is visible in Figure 4(3) at an air flow rate of $\approx 3\,\mathrm{L\,min^{-1}}$.

A comparison of the three cases at a water flow rate of $28\,\mathrm{L\,min^{-1}}$ (2), (3), and (4) shows that the phase distributions (a), (b), and (d) show very reproducible pressure levels and stopper positions. In case of the phase distribution (c), the behavior differs as shown in Figure 4(4) at an air flow rate from 2.2 to $2.9\,\mathrm{L\,min^{-1}}$.

In all presented cases in Figure 4 and 5, the difference between different water and air flow rates at constant phase distribution is small compared with the differences between different phase distributions at constant air and water flow rates.

5. Conclusion

The measurement results presented in this article include four different phase distributions. These phase distributions are a result of the air and water flow rate, the wetting conditions, and the history of the flow (increasing or decreasing air flow rate). Up to three different phase distribution patterns have been observed at distinct water and air flow rates. Accordingly, the effect of phase distribution on the stopper lift and the stopper tip pressure can be isolated. This impact is shown to surpass the effect of the water flow change from 28 to $32\,\mathrm{L\,min^{-1}}$.

The range of contact angles covered by the experiments reaches from 78° to 101°. These changes are sufficient to change the phase distribution in the SEN. Contact angle changes of this order of magnitude might be encountered in the steel plant due to a change in the cast steel grade or the growth of clogging material. This in turn leads to a significant change in the relation of stopper lift to liquid steel flow, which could affect the mold-level control algorithm. In addition, the resulting bubble size distribution reaching the mold could be affected as well.

Three of the four phase distribution patterns lead to a completely wet SEN wall. These phase distributions can easily be distinguished in a transparent water model, as the difference is visible. They are much harder to detect in liquid metal experiments or in the real caster. There the liquid is opaque, so even with a transparent setup only gas volumes attached to the walls can be seen. It is as well difficult to detect the different phase distributions with electromagnetic measurement systems as they mainly measure the outer shape of the liquid metal. Accordingly, the results presented in this paper can help to detect the different phase distributions based on the stopper lift and the stopper feeding pressure.

Supporting Information

Supporting Information is available from the Wiley Online Library or from the author.

Acknowledgements

The authors gratefully acknowledge the funding support of K1-MET GmbH, metallurgical competence center. The research program of the competence center K1-MET was supported by Competence Center for Excellent Technologies (COMET), the Austrian program for competence centers. COMET is funded by the Federal Ministry for Transport, Innovation and Technology, the Federal Ministry for Science, Research and Economy, the province of Upper Austria, Tyrol, and Styria, and the Styrian Business Promotion Agency.

Conflict of Interest

The authors declare no conflict of interest.

Data Availability Statement

The data that support the findings of this study are available in the supplementary material of this article.

Keywords

contact angles, hysteresis, one-third water models, phase distributions, submerged entry nozzles

Received: December 21, 2021
Revised: June 14, 2022
Published online: July 14, 2022

[1] B. G. Thomas, *Steel Res. Int.* **2018**, *89*, 1700312.
[2] H. Yang, H. Olia, B. G. Thomas, *Metals* **2021**, *11*, 116..
[3] R. Liu, B. G. Thomas, J. Sengupta, in *Model. Cast. Weld. Adv. Solid. Proc. (MCWASP) XIII*, Institute of Physics Publishing (IOP), Bristol, England **2012**.
[4] T. Hbiki, H. Goda, S. Kim, M. Ishii, J. Uhle, *Int. J. Heat Mass Transf.* **2004**, *47*, 1847.
[5] M. Ishii, S. Paranjape, S. Kim, X. Sun, *Int. J. Multiphase Flow* **2004**, *30*, 779.
[6] O. Kashinsky, P. Lobanov, M. Pakhomov, V. Terekhov, *Int. J. Heat Mass Transfer* **2006**, *49*, 3717.
[7] D. N. Mena, *Master Thesis*, The Pennsylvania State University **2016**.
[8] M. Milan, N. Borhani, J. Thome, *Int. J. Multiphase Flow* **2013**, *56*, 126.
[9] S. Qiao, D. Mena, S. Kim, *Nucl. Eng. Des.* **2017**, *312*, 375.
[10] M. Saeedipour, S. Pirker, in *Proc. 9th Int. Conf. Mod. Sim. Met. Proc. Steelmaking*, ASMET, Austrian Society for Metallurgy and Materials, Leoben, Austria **2021**, p. 242–250.
[11] S. Higson, P. Drake, U. Sjöström, *Improvement in Cast Product Quality by the Visualization and Control of the Steel Flow Pattern in the Tundish Pouring Nozzle (SEN/SES)*, EU Book shop, EUR 21247 EN, Luxembourg, **2005**.
[12] N. Terzija, W. Yin, G. Gerbeth, F. Stefani, K. Timmel, T. Wondrak, A. Peyton, *Flow Meas. Instrum.* **2011**, *22*, 10.

[13] H. Bai, B. G. Thomas, *Metall. Mater. Trans. B* **2001**, *32*, 269.
[14] K. Timmel, T. Wondrak, S. Eckert, *IOP Conf. Ser.: Mater. Sci. Eng.* **2018**, *424*, 012032.
[15] K. Timmel, N. Shevchenko, M. Röder, *Metall. Mater. Trans. B* **2015**, *46B*, 700.
[16] M. Ratajczak, D. Hernández, T. Richter, D. Otte, D. Buchenau, N. Krauter, T. Wondrak, *IOP Conf. Ser.: Mater. Sci. Eng.* **2017**, *228*, 012023.
[17] J. Eck, *Master-Thesis*, Lulea University of Technology, **2019**.
[18] G. Holzinger, M. Thumfart, *Steel Res. Int.* **2019**, *90*, 1800642.
[19] S. Hänsch, I. Evdokimov, F. Schlegel, D. Lucas, *Chem. Eng. Sci.* **2021**, *244*, 116807.
[20] G. Tryggvason, S. Dabiri, B. Aboulhasanzadeh, J. Lu, *Phys. Fluids* **2013**, *25*, 031302.
[21] *ANSYS Fluent User's Guide* **2021**, *R1*, p. 2511.
[22] M. Thumfart, *Master-Thesis*, JKU Linz, **2008**.
[23] A. Karasangabo, *PhD-Thesis*, MUL Leoben **2009**.